Renewable Energy 71 (2014) 598–608

Contents lists available at ScienceDirect

Renewable Energy

journal homepage: www.elsevier.com/locate/renene

Wave energy resources near Hot Springs Cove, Canada

Clayton E. Hiles [a, *], Bradley J. Buckham [b], Peter Wild [b], Bryson Robertson [b]

[a] Cascadia Coast Research Ltd., 26 Bastion Square, Third Floor – Burnes House, Victoria, BC V8W1H9, Canada
[b] University of Victoria, Department of Mechanical Engineering, PO Box 3075 STN CSC, Victoria, BC V8W 3P6, Canada

ARTICLE INFO

Article history:
Received 17 August 2013
Accepted 11 June 2014
Available online

Keywords:
Wave power
Wave resource assessment
Site selection
Near-shore
Wave model
Vancouver Island

ABSTRACT

Hot Springs Cove on the West Coast of Vancouver Island, Canada is an off-grid community of approximately 80 residents reliant on diesel fuelled electricity generation. Recent concerns with on site diesel based electricity generation have prompted interest in renewable alternatives, including wave energy. To help evaluate the feasibility of deploying ocean wave energy conversion technologies near Hot Springs Cove, a preliminary assessment of the area's near-shore wave energy resources was performed. A near-shore wave model, utilizing a transfer function approach, was used to estimate wave conditions from 2005 to 2013 at a 3 h time-step. Spectral wave data from NOAA's Wavewatch3 model were used as model input boundary conditions. The wave spectra resulting from the near-shore model were parameterized to indicate the magnitude and frequency-direction distribution of energy within each sea-state. Yearly mean values as well as monthly variation of each of the spectral parameters are plotted to indicate the spatial variation of the wave climate. A site in 50 m of water, appropriate for a 2-body point absorber, was selected based on a number of generic constraints and objectives. This site is used to illustrate the temporal variation of the spectral parameters within each month of the year. The average annual wave energy at the reference location is 31 kW/m, with a minimum (maximum) monthly average of 7.5 (60.5) kW/m. The magnitude of this resource is significantly greater than other high profile sites in Europe such as the WaveHub and EMEC, and indicates that the Hot Springs Cove region may be a good candidate for wave energy development.

1. Introduction

Marine renewable wave energy is increasingly recognized as a viable source of energy for electricity production. The deployment of wave energy conversion (WEC) technologies for electrification of off-grid coastal communities is viewed as particularly attractive. These communities are typically close to energetic ocean waves and already paying high electricity prices for on-site generation.

One such community is Hot Springs Cove on the West Coast of Vancouver Island, Canada (see Fig. 1). This community of approximately 80 residents is completely reliant on imported diesel fuel for electricity generation. The high cost, cost uncertainty and environmental damage associated with diesel based electricity generation have prompted interest in renewable alternatives, including wave energy. To assess the feasibility of providing wave energy generated electricity to Hot Springs Cove an assessment of the regional wave energy resources was required.

The present study seeks to build an understanding of the wave resource in the region by performing a high resolution multi-year hind-cast of wave conditions by using a validated numerical model which provides spectral wave estimates over the entire region of interest. For near-shore regional assessments such as this it is typical to use a nesting approach where the regional model is driven at an ocean boundary with wave conditions sourced from an ocean scale model [1–5].

There are two predominant methodologies for modelling near-shore wave resources. The first involves binning the off-shore wave climate into an array of parameterized sea-states [1,2,6]. The near-shore model is run for each binned sea-state state. Then, based on the occurrence of each off-shore sea-state, the wave climate near-shore can be determined. The advantage of this method is that the number of runs is limited by the range of parameterized sea-states at the study site. When many years of wave conditions are computed this approach can reduce the required simulation effort by several orders of magnitude. The disadvantage of this method is that the sea-states must be parameterized, thereby neglecting much detail in the wave spectrum that is important for determining WEC performance. Additionally this method has only limited

* Corresponding author.
E-mail addresses: clayton@cascadiacoast.com (C.E. Hiles), bbuckham@uvic.ca (B.J. Buckham), pwild@uvic.ca (P. Wild), bryson@uvic.ca (B. Robertson).

http://dx.doi.org/10.1016/j.renene.2014.06.020
0960-1481/

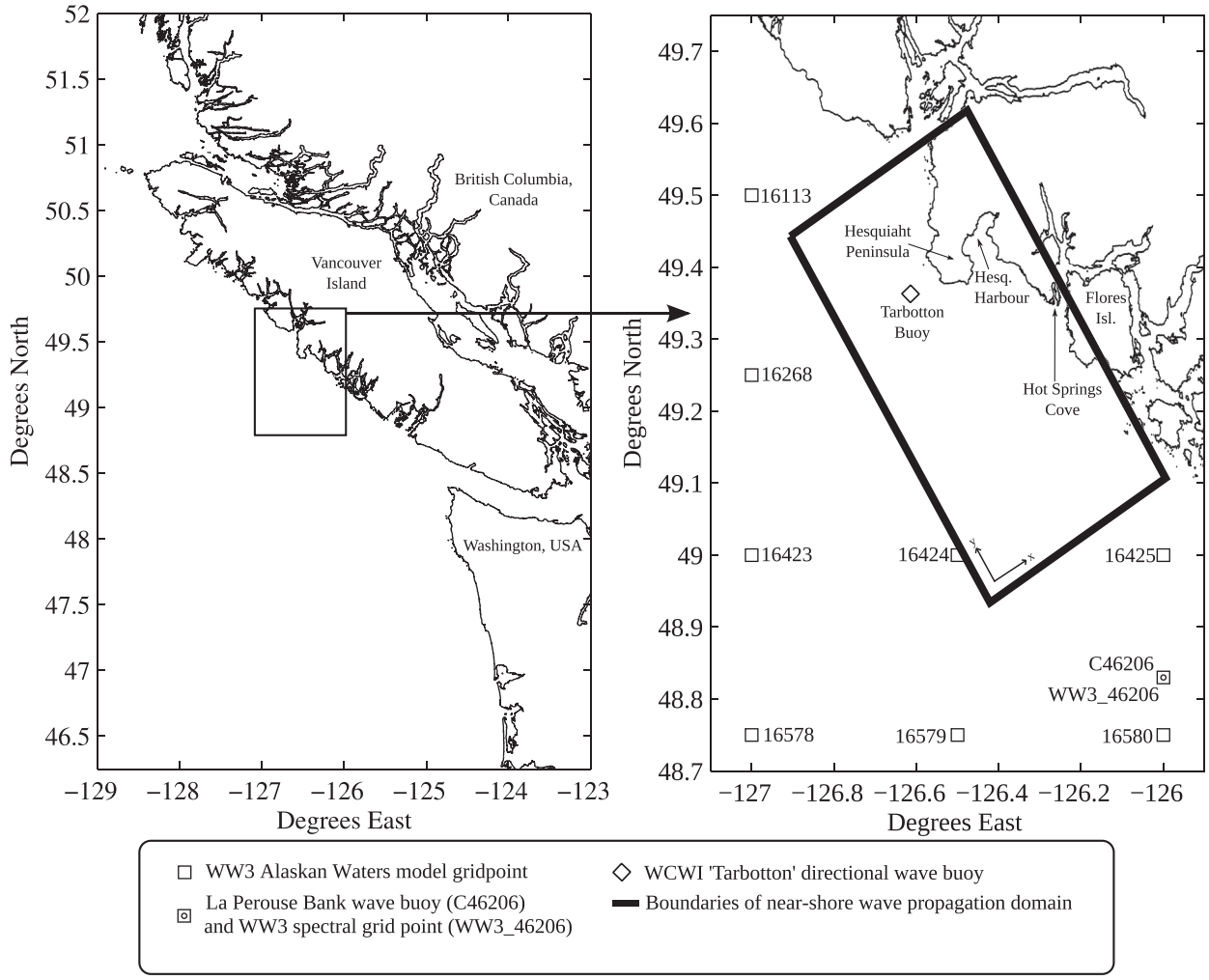

Fig. 1. [left] Shorelines of Washington and B.C.; rectangle indicates inset. [right] Inset showing locations of Hot Springs Cove, WW3 Alaskan Waters Model grid points, buoys and boundaries of the wave propagation model.

ability to consider non-wave boundary conditions such as winds, tides and currents.

The second method for modelling the wave resource is a time-series approach. Wave conditions are simulated at discrete time-steps over a long hind-cast period and the time-series results are analysed to produce summary statistics [3–5]. The advantage of this method is that boundary conditions are specific to each time step so they may be as detailed as required. Depending on the abilities of the model, non-wave boundary conditions such as winds, tides and currents may be naturally included. The disadvantage of this method is the significant computational expense. Simulating 10 years of wave conditions at 3 h intervals would require 292,220 simulations.

The transfer function approach taken in this study is a hybrid of the above methodologies [8]. A linear wave model is used to pre-compute the response of the model domain to each component of a discritized directional wave spectrum applied at the off-shore boundary. Since the model is linear, each component is computed only once using a unit wave amplitude. Each model result can then be used as a transfer function for that component of the wave spectrum. The resultant near-shore wave amplitude is simply the input off-shore wave amplitude multiplied by the transfer function. With the amplitude of each wave component calculated, the spectrum can be recovered by converting the amplitude of each component back to variance density and summing the results.

The advantage of the transfer function approach is that it allows the wave spectrum at any point throughout the modelled domain to be calculated quickly for any arbitrary input wave spectrum. In this way wave conditions can be calculated over many years very quickly without neglecting detail in the wave spectrum. The downside of this approach is that non-linear physics such as wind generation cannot be included, but, it will be shown in Sections 3 and 4 these effects are generally of secondary importance in the study area.

This paper describes the set-up, validation, and results from a 8 year hind-cast of wave conditions in the coastal region surrounding Hot Springs Cove. The study area and general characteristics of the wave climate are described in Section 2. The study methodology including the wave modelling software, modelling approach, boundary conditions, computational grid and techniques for characterization of model results are covered in Section 3. The model is validated to measurements from a fully directional wave buoy in Section 4. The representativeness of the hind-cast period of the long-term wave climate is explored in Section 5. The hind-cast results are presented and discussed in Section 6. The spatial distribution of the resource is considered first using a number of contour maps. A reference site, appropriate for a two-body point absorber technology, is then selected through the application of a number of generic WEC constraints and objectives. That site is used to illustrate the temporal distribution of the resource through each

month of the year. The joint probability of important wave parameters are presented and discussed and the yearly average wave energy is compared to other well known WEC test sites. Concluding remarks are provided in Section 7.

2. Setting

Hot Springs Cove is located at 49.36N, 126.26W, just east of Hesquiaht Peninsula and Hesquiaht Harbour and west of Flores Island (see Fig. 1). The wave climate in this region is most powerful in the winter months, and least powerful during the summer months. During the winter, swell is typically generated by large storms in the North Pacific and arrives from the north–westerly direction, though, significant wave systems can also be generated more locally by high winter winds. Hesquiaht Harbour, and to a lesser extent the entrance to Hot Springs Cove, are protected from strong north–westerly waves by Hesquiaht Peninsula. During the summer waves are typically generated by low magnitude local winds. In addition, during the summer there is often a long period swell arriving from the south. This swell originates in winter storms in the Southern Ocean. As a result of this southern swell contribution, wave spectra in the summer are often double peaked.

3. Methodology

This resource assessment employs a one-way nesting of wave models: essentially the results from a larger ocean-scale model are used as boundary conditions to drive a smaller, shelf-scale wave model. This approach was selected so that eight years of off-shore wave data available from the National Oceanic and Atmospheric Administration (NOAA) could be leveraged to quickly produce a statistically robust database of near-shore wave estimates covering March 2005 to February 2013.

3.1. Wave modelling software

REF/DIF-1 is a phase resolved monochromatic wave modelling software based on the *mild-slope equation* [7]. In this work REF/DIF-1 was used in linear mode to calculate wave propagation. The *wide angle approximation* was used to allow propagation of waves $\pm 75^\circ$ to the boundary normal. The wave spectrum was binned at a constant 15° width in direction and at a variable 0.0955 f width in frequency (where f is the bin-centre frequency). A smoothing filter available in REF/DIF was applied to the results to avoid the artificially narrow directional spread of wave energy.

3.2. Transfer function method

To model irregular waves a transfer function approach is used [8]. Each variance density bin in the input wave spectrum is first converted to a monochromatic wave using Eq. (1). Since the model is linear, the propagation of each wave component is pre-computed only once using a unit wave amplitude. Each model result can then be used as a transfer function for that component of the wave spectrum. The resultant near-shore wave amplitude is computed as the product of the input off-shore wave amplitude and the appropriate transfer function. The wave period does not change during wave propagation and resultant wave direction does not vary with wave amplitude.

With this approach the wave height, period and direction for each of the monochromatic components derived from the input wave spectrum can be calculated at every grid location in the model. The near-shore wave spectra can be recovered by converting each of the monochromatic waves back to variance density. Appropriate portions of the variance density corresponding to each discrete component are then summed into the appropriate spectral bins to yield the variance density spectrum. This re-allocation of variance is required because wave components tend to migrate through directional bins during the propagation process.

Significant computational resources are needed to model waves at the spatial and spectral resolution appropriate for the near-shore region. The transfer function method used here allows results to be generated with minimal model runs, in this case just 275. Computational efficiency was important for this work in order to maintain high spatial and spectral resolution over the hind-cast period while keeping the problem tractable without the need for supercomputing facilities.

3.3. Limitations of transfer function method

The wave model employed in this work is linear. Linearity of wave components is assumed in the spectral representation of waves, but is not valid under all conditions. In deep to intermediate depths and with low wind forcing, linear wave theory provides a good representation of waves. Linear wave theory breaks down where waves become very steep: during generation due to wind forcing, in very shallow water due to interactions with the sea floor and also in the presence of strong currents. Non-linear interactions also facilitate the transfer of energy from high to low frequencies in developing seas.

Most spectral wave models handle the non-linear wave physics by including *source terms* in the computations which facilitate the transfer of energy from the wind to waves and between wave components. The current model does not include source terms so physics of wave generation, white-capping and wave–wave interactions are not captured.

Wave generation and white-capping are both products of wind forcing. The relative effect of omitting wind forcing was evaluated by examining 25 years of wind and wave data available from buoy C46206 (Fig. 1). When the wave phase speed approaches the wind speed, the relative wind speed approaches zero and no longer contributes to wave generation and the wave spectrum is deemed *fully developed* [9]. By this criteria the sea is fully developed at buoy C46206 95% of the time. Only 0.02% of the time does the wind speed exceed double the wave phase speed. This means that even when winds are causing local generation, the contribution is small.

The current model also does not account for bottom friction. Numerical experiments by Folley and Whittaker (2009) suggest that bottom friction results in about a 10% loss of energy between the 50 m and 10 m contours [10]. This may mean that the current model slightly over estimates wave energy in shallow waters, but should not significantly impact results in waters greater than 40 m (the depth constraint required for the representative two-body point absorber considered). A spectral depth-limited breaking scheme is not used in the current work, so all results shallower than 16 m are masked to eliminate any erroneous results.

Supporting this model configuration is the work of Garcia-Medina et al. (2013), who examined a range configurations for a near-shore wave model covering the inner shelf of the US Pacific Northwest, not far from the study area [11]. For their model they show that wind-generation, bottom friction and white-capping play a secondary role to refraction and shoaling in influencing the wave conditions and the exclusion of these physics does not significantly effect estimates of bulk parameters.

3.4. Computational grid and bathymetry

This study used a regular, rotated computational grid of dimensions 66,800 × 36,700 m with 50 m node spacing for a total of 981,000 nodes. The high resolution of the grid is only made feasible by the efficiency of the transfer function approach.

Bathymetric data was obtained as a *xyz*-scatter from Canadian Hydrographic Service surveys. In total there were 480,000 soundings at varying density. The scatter data was linearly interpolated onto the computational grid (Fig. 2). REF/DIF requires at least 5 nodes per wave-length, and for shorter wavelength waves, the base computational grid was sub-sampled up to a maximum of 26 times (2 m resolution) at run time.

3.5. Wave boundary conditions

Directional wave spectra from the NOAA WW3 global mosaic model were used as a boundary condition for the REF/DIF model. NOAA WW3 model results are one of the only publicly available sources of directional wave spectra for the shelf seas of the West Coast of Canada and the most widely used for research of this type. Reanalysis results are available from February 2005 to 2013, but the NOAA only outputs spectral data at the locations of permanent wave buoys. The closest output location to the model domain boundary is at the location of buoy C46206, referred to here as WW3_46206 (See Fig. 1). The variance density spectra ($S(\theta,f)$) from WW3_46206 contain 24 bins of 15° width in the direction dimension and 25 bins of 0.0955 f Hz width in the frequency dimension (0.04–0.41 Hz).

3.5.1. Local validation of WW3

Data from WW3_46206 was locally validated against measurements made at buoy C46206 which is coincident in space (See Fig. 1). This buoy is owned and maintained by Environment Canada (EC). The WW3 results were compared to the buoy data based on the bulk spectral parameters *significant wave height* (H_{m0}) and *peak period* (T_p). Only buoy data assigned by EC an IGOSS quality control flag of 1 (*QC has been performed*: *record appears correct*) were used [12]. Table 1 shows bias (b), rms error (e_{rms}) and correlation coefficient (r) for each parameter for the 6 years of coincident data available (see Ref. [11] for equations). Note that buoy C46206 does not measure directionality.

Table 1 shows that the WW3 model has reasonable accuracy in predicting the bulk parameters at this location. WW3 slightly over-predicts H_{m0}, but e_{rms} and r are good. The bias (b) of T_p is low and the reported e_{rms} and r are indicative of the unstable nature of the peak period values [13].

3.5.2. Transfer of wave data to model boundary

WW3_46206 is about 25 km from the model boundary. To ensure that data from WW3_46206 is representative of wave conditions at the model boundary, it was compared to the parametric data available at grid point 16,424 of the Alaskan Waters Model (AKW16424), on the near-shore model boundary (see Fig 1). Table 2 shows bias and rms error for the 3 years of coincident data available. Note that only the parameters H_{m0}, T_p and θ_p (*primary wave direction*) are available at AKW16424.

The bias of T_p and θ_p are low in magnitude, within the bin resolution. The −0.12 m bias in Ref. H_{m0} (indicating under-prediction) is low and opposite in sign to the bias between WW3_46206 and buoy C46206. As in the previous section, r for T_p and θ_p is relatively low but this is expected due to the unstable nature of 'peak' parameters. While there are discrepancies between WW3_46206 and the computational boundary, these are minimal and on the same order as the resolution of each computation bin.

Given the above analysis in Sections 3.5.1 and 3.5.2, the data from WW3_46206 was used directly as a boundary condition to wave propagation model without any correction factors. It is acknowledged that these boundary conditions are not ideal, but the best currently available. It is believed that the insights yielded by the use of full directional spectra (as opposed to synthetic spectra based on H_{m0} and T_p) outweigh the uncertainly introduced by using data from a location 25 km away. Additionally, due to the transfer function approach used, the model developed here may be reused without significant additional effort once better boundary condition data becomes available.[1]

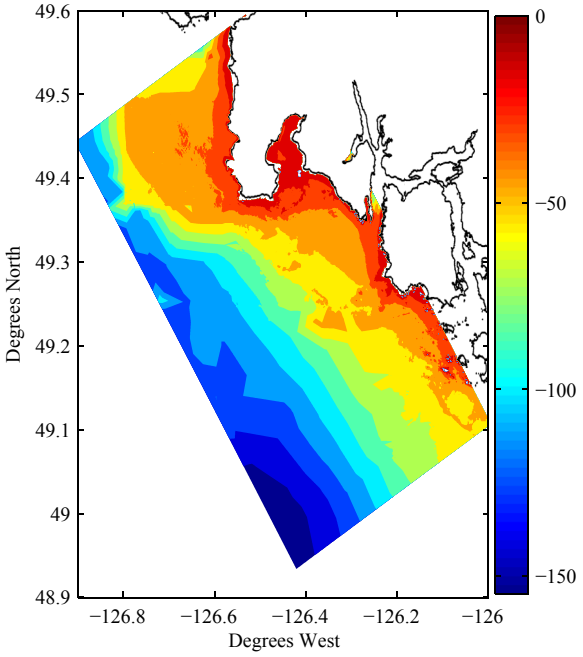

Fig. 2. Bathymetric contours in the near-shore propagation model domain.

Table 1
Statistics comparing WW3_46206 to buoy measurements at C46206.

	b	e_{rms}	r
H_{m0} (m)	0.17	0.51	0.92
T_p (s)	0.23	2.7	0.55

3.5.3. Boundary condition setup

This spectral discretization of the WW3 boundary conditions (24 bins in the direction dimension and 25 bins in the frequency dimension [0.04–0.41 Hz]) was retained in the near-shore model. Only components coming from directions between 112° and 337° propagate into the model domain from the boundary, so the remainder of the spectrum was not included in the near-shore model.

For propagation of each component in REF/DIF-1, spectral density was converted to wave amplitude by:

$$A_{i,j} = \sqrt{2S\left(\theta_i, f_j\right)\Delta\theta_i\Delta f_j} \tag{1}$$

where A is wave amplitude, $\Delta\theta$ is direction bin-width, Δf is frequency bin-width and i and j are indices of the direction and frequency bin.

3.6. Characterization of results

Using the methods described in Section 3, the near-shore model yields fully directional spectra throughout the domain. The spectra are parameterized to facilitate the communication of the

[1] Continuing efforts of this research group include the development of a regional shelf-scale spectral wave model for the Canadian West Coast.

Table 2
Statistics comparing WW3_46206 to AKW16424.

	b	e_{rms}	r
H_{m0} (m)	−0.12	0.27	0.98
T_p (s)	0.73	2.3	0.67
θ_p (°)	5	30	0.50

magnitude and frequency-direction distribution of wave energy within each sea-state.

3.6.1. Parameterization of spectra

Wave spectra are parameterized for characterization in a manner similar to the Draft Specification for Wave Resource Assessment currently in preparation by the International Electrotechnical Commission (IEC) Technical Committee 114 [14]. These methods are already in use by others [5,15]. Standard parameters used for characterization include *omni-directional wave power* (J), *significant wave height* (H_{m0}), *energy period* (T_e) and *spectral moments* (m_n), definitions for which can be found in most ocean engineering texts (e.g Ref. [9]).

The frequency and direction distribution of energy within the wave spectrum were additionally parameterized using the *spectral width* (ε_0), the *direction and magnitude of maximum directionally resolved wave energy* (θ_j,J_{θ_j}) and the wave power *directionality coefficient* (d). The equations for these quantities are provided in Eqs. (2)–(5).

$$\varepsilon_0 = \sqrt{\frac{m_0 m_2}{m_1^2} - 1} \tag{2}$$

$$J_\theta = \rho g \sum_j C_{g_j} S_{i,j} \Delta f_j \Delta\theta_i \cos(\theta - \theta_j)\delta \tag{3}$$

$$\delta = \begin{cases} 0 & \text{if } \cos(\theta - \theta_j) < 0; \\ 1 & \text{if } \cos(\theta - \theta_j) \geq 0; \end{cases}$$

where θ is the direction of resolution and C_g is the group velocity.

$$J_{\theta_j} = \max(J_\theta) \tag{4}$$

where θ_j is the direction corresponding to $\max(J_\theta)$.

$$d = J_{\theta_j} \Big/ J \tag{5}$$

3.6.2. Spatial characterization

The parameters derived from the wave spectrum were characterized based on their annual mean values, monthly variation and yearly maximum. Monthly variation is defined based on the maximum and minimum of the monthly average values.

Table 3
Validation statistics comparing near-shore model results to WCWI buoy 'Tarbotton'.

	b	e_{rms}	r
H_{m0} (m)	−0.06	0.34	0.90
T_e (s)	0.6	1.3	0.74
T_p (s)	1.3	3.9	0.40
θ_p (°)	9	39	0.40
J (kW)	−1.3	10	0.89
J_{θ_j} (kW)	−0.3	9	0.89
θ_j (°)	7	22	0.78
ε_0	−0.01	0.09	0.39
d	0.08	0.11	0.54

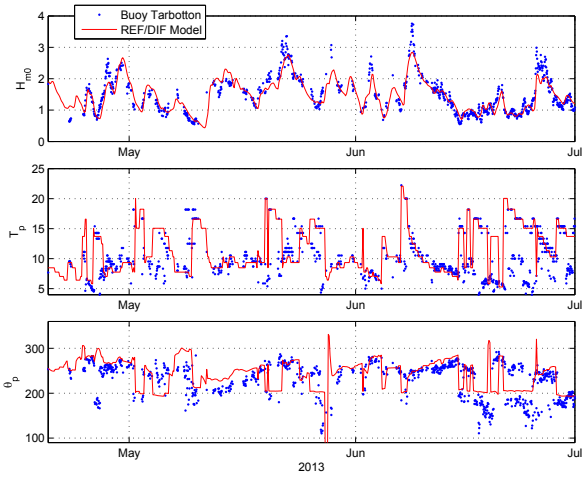

Fig. 3. Time series comparison of measured and modelled H_{m0}, T_p and θ_p at buoy *Tarbotton*.

$$\mathrm{MV}(p) = p_{\max} - p_{\min} \tag{6}$$

where $p_{\max}$ and $p_{\min}$ are the maximum and minimum of the monthly mean values of parameter p.

3.6.3. Temporal characterization

A reference location is selected in the area of interest near Hot Springs Cove. Using this reference location the variability of the wave climate during each month is characterized by the mean, standard deviation, 50th, 10th and 90th percentiles of J, H_{m0}, T_e and ε_0.

4. Near-shore model validation

As part of the work associated with this project, a directional wave measurement buoy, identified as 'WCWI Tarbotton' on the Automatic Identification System, has been deployed near the Hesquiaht Penninsula. The buoy is deployed at 49.3518N −126.6066E in about 42 m of water (see Fig. 1) and will be kept at this location through 2015. Real-time measurements from the buoy can be viewed at www.uvic.ca/wcwi .

Directional spectra recovered from the buoy for the period of April–December 2013 have enabled the validation of the wave model. Table 3 below gives the bias and rms error of the model compared to the measurements in terms of H_{m0}, T_p, θ_p as well as T_e, ε_0, J, J_{θ_j}, d and θ_j as described in Section 3.6.1.

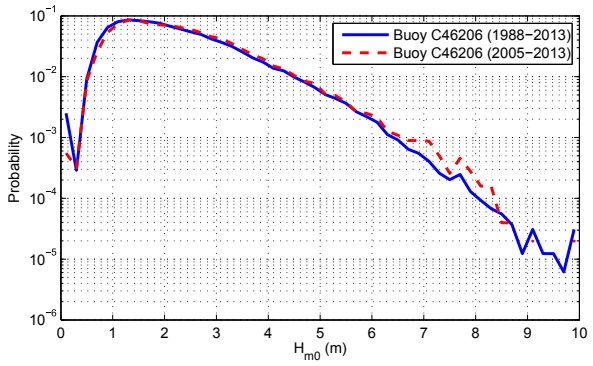

Fig. 4. Probability density functions for H_{m0} at buoy C46206 (0.2 m H_{m0} bins).

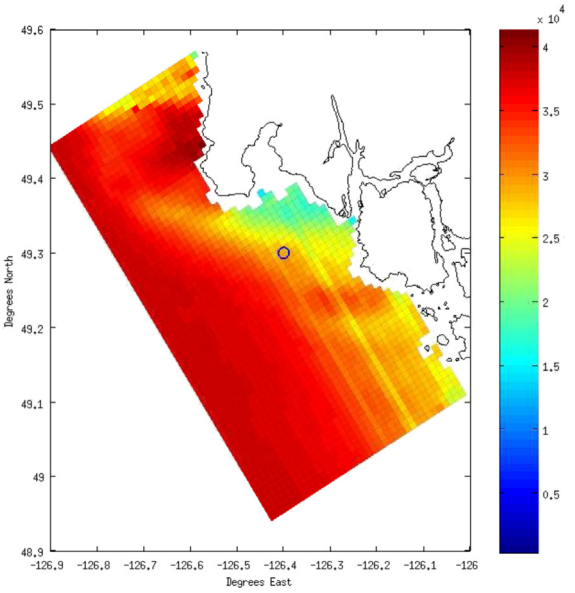

Fig. 5. Colour contours of yearly average wave power, J (W/m).

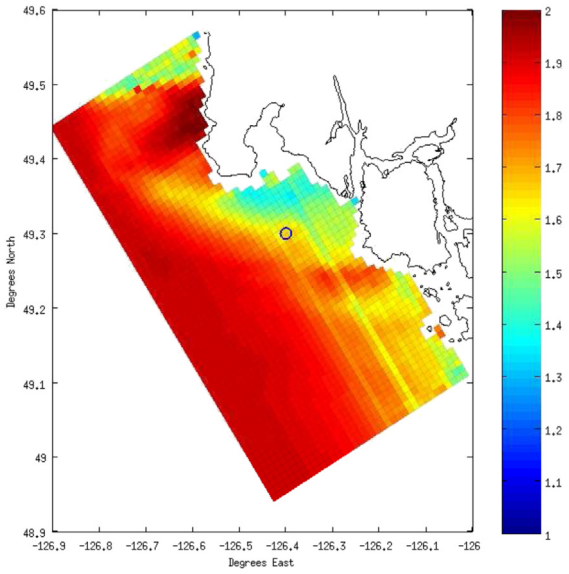

Fig. 7. Monthly variability significant wave height, H_{m0} (m).

The model shows very low bias in Refs. H_{m0}, T_e, T_p and θ_p. High e_{rms} and moderate r in Refs. T_p and θ_p are notable, but both are similar to the error in the input boundary conditions. Furthermore, the unsteady nature of these 'peak' parameters makes absolute agreement difficult [13]. Fig. 3 shows a time-series comparison of measured and modelled H_{m0}, T_p and θ_p.

Of the wave resource characterization parameters, only d, which depends on the accuracy of both J_{θ_j} and J shows significant bias. The positive bias in d results from clipping of the spectra at the off-shore boundary: only half of the directional bins in the incident wave spectrum can be propagated into the near-shore model (components travelling sea-ward through the off-shore boundary are not included). The buoy spectra obviously contain all directional bins.

The remainder of these parameters show very low b, low e_{rms} and high r, lending confidence to analysis presented in Section 6.

5. Hind-cast representation of long term wave climate

The hind-cast is performed over eight years, March 2005 to February 2013. It bears consideration how well this period represents the long-term wave climate. This was explored using measurements from buoy C46206, available from 1988 through 2013. The probability density function (pdf) of H_{m0} was calculated for both the entire C46206 data-set (1988–2013) and for a sub-set covering only the hind-cast period (2005–2013). A good fit of the shorter duration pdf to the longer indicates that the full range of possible wave conditions are represented within the 2005–2013 hind-cast period.

Fig. 4 shows the two pdfs. The pdf for the hind-cast period closely follows the pdf for the entire data-set up to about $H_{m0} = 7$ m, beyond which there appears there is insufficient data to define the pdf. Almost all occurrences are captured in the region

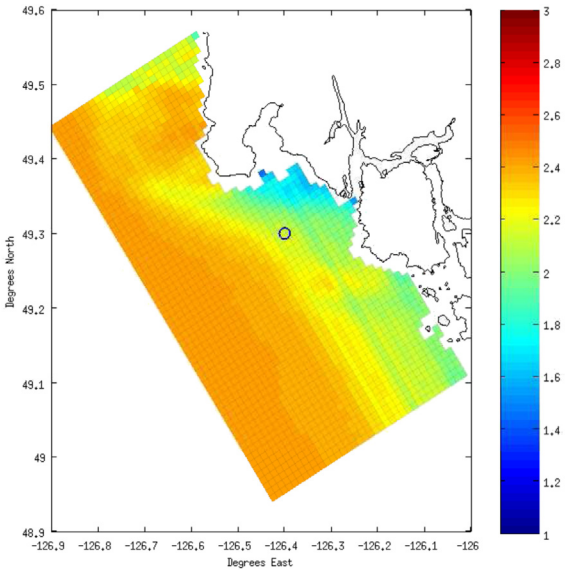

Fig. 6. Yearly average significant wave height, H_{m0} (m).

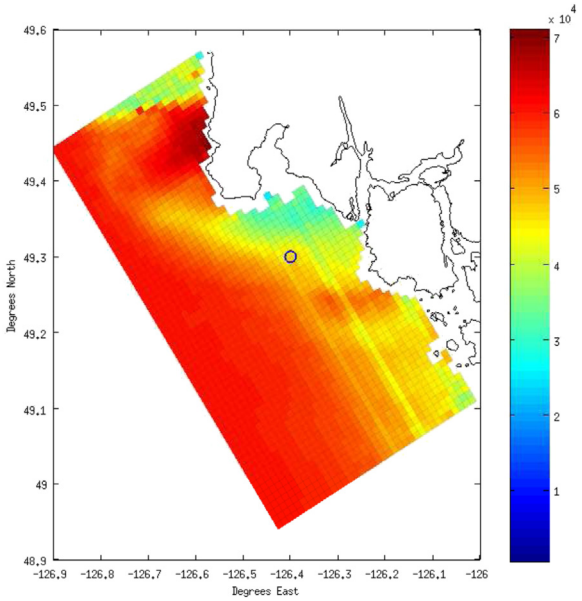

Fig. 8. Monthly variability of wave power, J (W/m).

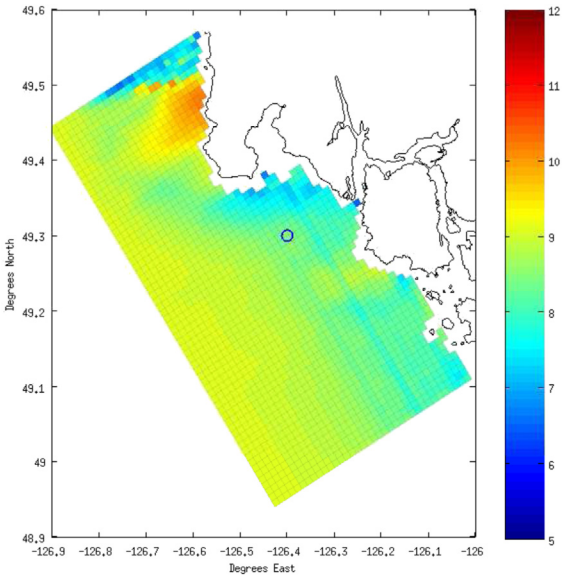

Fig. 9. Maximum significant wave height, H_{m0} (m).

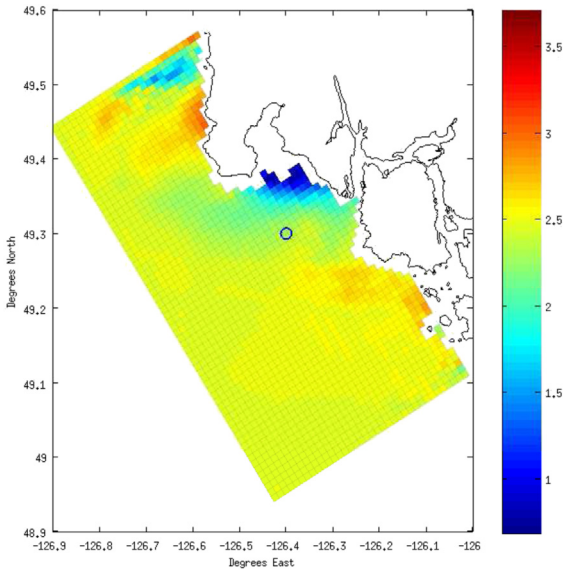

Fig. 11. Monthly variability energy period, T_e (sec).

where the pdfs match; waves H_{m0}< 7 m account for 99% of wave energy. This analysis suggests that in general the hind-cast period is representative of at least 1988–2013, but the hind-cast period might not capture the most extreme wave conditions.

6. Results and discussion

This section examines the results of the eight year wave hind-cast. The discussion is divided into four sections examining: the spatial variability of wave parameters, the temporal variability of wave parameters, the most probable and most energetic sea-states and a comparison to existing wave energy test facilities.

6.1. Spatial variation in study area

Plots of the yearly average and monthly variability can be found in Figs. 5–16. For clarity the results are decimated down to 1 km by 1 km spacing. Note that the accuracy of the model may be degraded near the lateral model boundaries due to lack of wave boundary conditions.

The plots of average J and H_{m0} (Figs. 5 and 6) show a characteristic distribution of energy/height. Shallower waters east of Hesquiaht Penninsula cause waves propagating towards the shore to refract northwards and concentrate on the west-facing shore of the Peninsula. Similarly, wave refraction causes the concentration of wave energy in the shallower waters off Flores Island (49.25N–126.3E). In the area between Hesquiaht Peninsula and Hot Springs Cove, outside the entrance of Hesquiaht Harbour, refraction and sheltering causes the divergence of wave energy and so lower wave power and height.

The maximum monthly average of H_{m0} (Fig. 7) is up to 2 m larger than the minimum; correspondingly the maximum monthly average of J (Fig. 8) is up to about 60 kW greater than the minimum. The maximum H_{m0} is about 9 m in most of the domain and down to

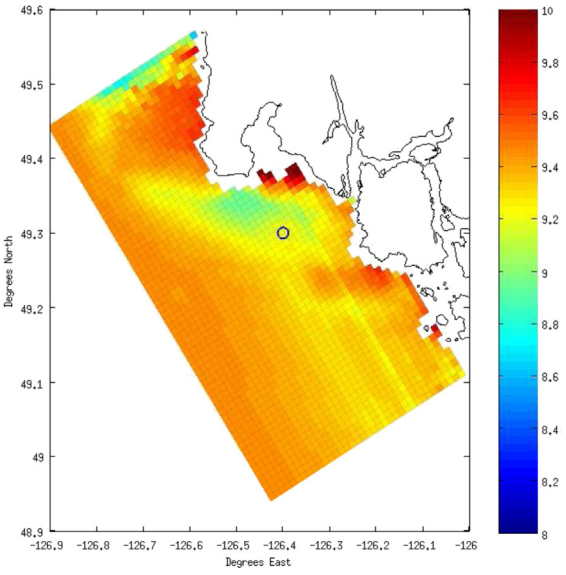

Fig. 10. Yearly average energy period, T_e (sec).

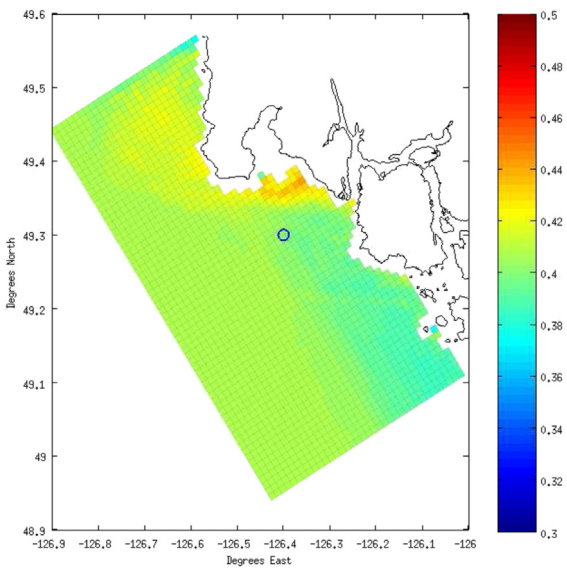

Fig. 12. Yearly average spectral width, ε_0.

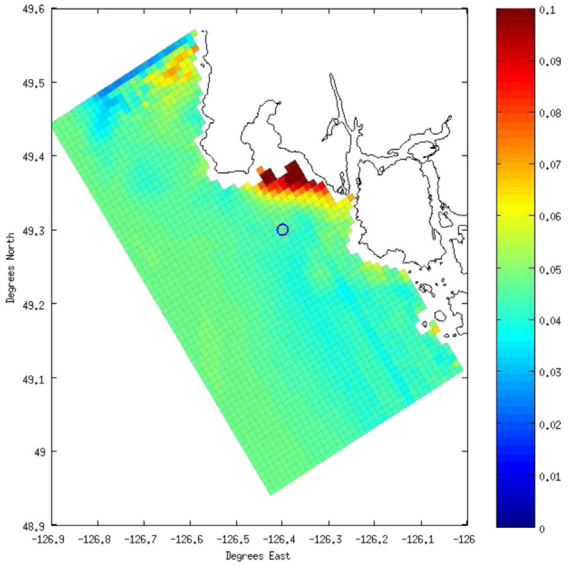

Fig. 13. Monthly variability of spectral width, ϵ_0.

about 7 m around the entrance of Hesquiaht Harbour (Fig. 9). Though average H_{m0} is lower at the entrance of Hesquiaht Harbour, the variability and the maximum H_{m0} are also lower. This may be advantageous for some WEC devices.

Yearly average T_e (Fig. 10) has strong spatial consistency, with an average between 8 and 10 s. Monthly variability (Fig. 11) is relatively low with a difference of 2.5 s in most of the domain. Interestingly, both T_e and the monthly viability of T_e are reduced outside the entrance of Hesquiaht Harbour. This occurs because energy in the long period/wave-length spectral components tend to be refracted away from this area, reducing the energy in the low frequency end of the spectrum. Inside the entrance of Hesquiaht Harbour is sheltered and so only reached by longer period waves which refract and diffract into this area; this sheltering effect results in a larger average T_e.

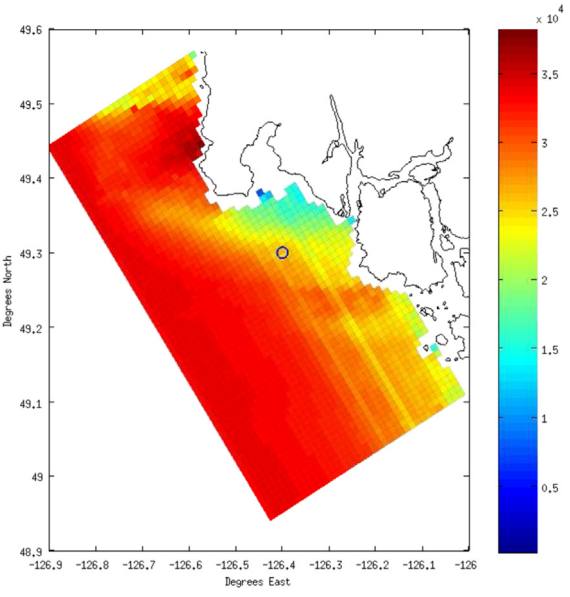

Fig. 14. Yearly average maximum directionally resolved wave power, J_{θ_j} (W).

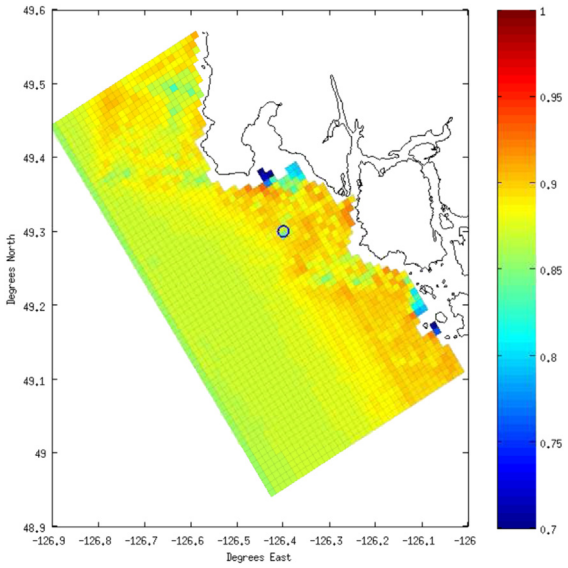

Fig. 15. Yearly average directionality coefficient, d.

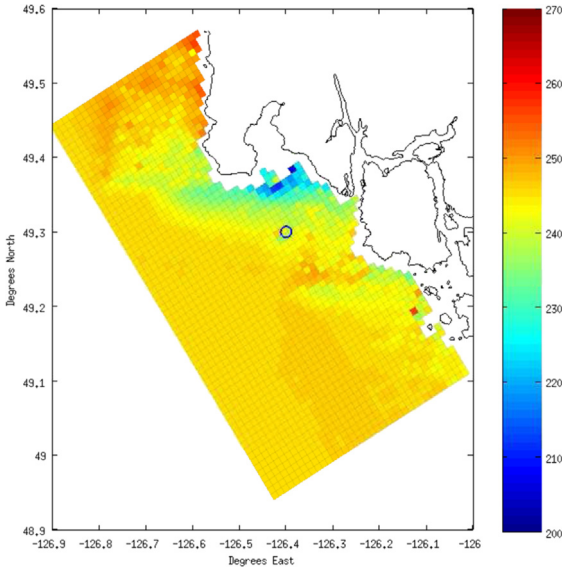

Fig. 16. Yearly average direction of maximum directionally resolved wave power, θ_j (deg).

Yearly average ϵ_0 (Fig. 12) also has strong spatial consistency with an average value of about 0.4 (indicating a relatively narrow spectrum). Monthly variability (Fig. 13) is low and spatially consistent, except at the entrance to Hesquiaht Harbour where wave shadowing and differing predominant directions throughout the year cause higher variability of ϵ_0.

Yearly average J_{θ_j} (Fig. 14) shows very similar spatial variation as yearly average J. In water deeper than 60 m, average d (Fig. 15)

Table 4
Siting objectives and constraints for a generic 2-body point absorbing WEC.

Parameter	Range/objective	Type
Depth (m)	40–80	Constraint
T_e (s)	7–10	Constraint
H_{m0} (m)	1–1.5	Constraint
J (kW)	maximize	Objective
Distance (km)	minimize	Objective

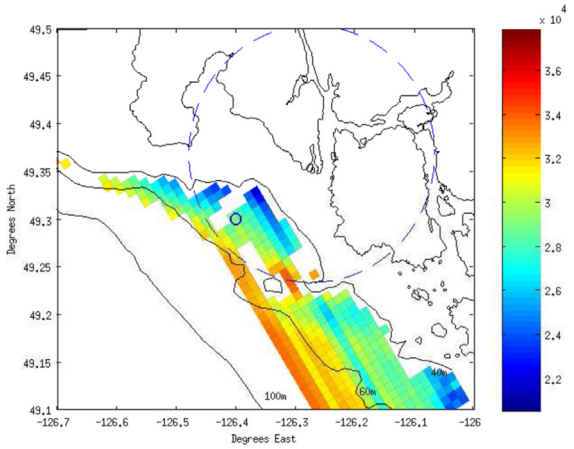

Fig. 17. Yearly average wave power, J (W/m), masked by site selection criteria. Dash-dot circle shows 15 km radius from Hot Springs Cove.

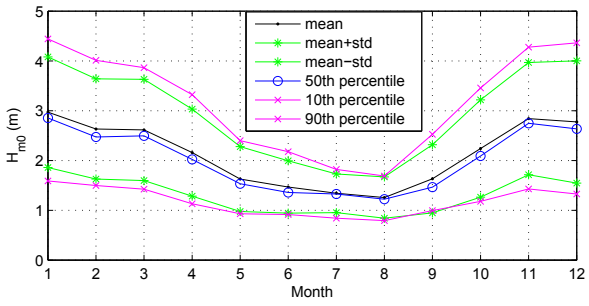

Fig. 18. Monthly variation of H_{m0} at reference location.

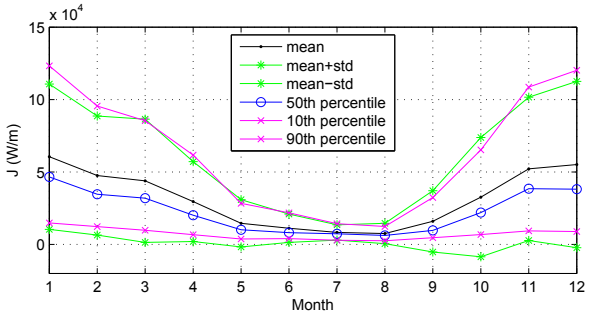

Fig. 19. Monthly variation of J at reference location.

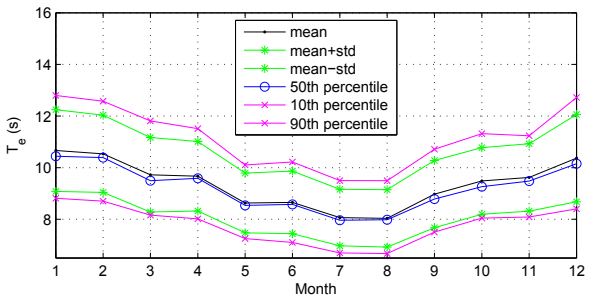

Fig. 20. Monthly variation of T_e at reference location.

shows that J_{θ_j} is spatially consistent at about 87% of J, and Fig. 16 indicates that θ_j averages about 250°. In waters shallower than 60 m, the d increases to about 90% and θ_j is more variable depending on the bathymetry. Recalling the model validation (Section 4), these values are likely optimistic by about 8% (likely less in depths less than 40 m). Still, these results represent a very low spreading of wave energy, which is a benefit to directional WEC technologies, which capture wave energy primarily from a single direction.

6.2. Temporal variation at reference location

To illustrate the temporal variation of the wave climate required that a representative point within the model be selected. This location was selected by considering a series of siting objectives and constraints for a generic 2-body point absorbing WEC as given in Table 4.

In Table 4 *Distance* refers to the distance from the site to Hot Springs Cove. The range of values of H_{m0} and T_e correspond to the most frequently occurring sea state. The possible deployment area is given by the intersection of these constraints. Fig. 17 shows colour contours of J over the possible deployment area. The site was selected from this area based on a qualitative trade off between distance to shore and average J. This trade off is illustrated in Fig. 17 with a 15 km radius dash-dot circle indicating the distance from Hot Springs Cove.

Through the application of this simple set of generic siting metrics, a reference location was determined to illustrate the temporal variation in the wave climate. The application of specific WEC siting metrics to the wave resource data provided in this study will allow project developers and WEC designers to locate and assess the performance of their devices in this region.

The selected site is at 49.3 N,−126.4°E in 50 m of water (shown with an 'o' in Figs. 5–17). For this location the monthly mean, mean ± one standard deviation, 10th, 50th and 90th percentile of J, H_{m0}, T_e and ε_0 are plotted in Figs. 18–21.

Fig. 18 shows there is strong variation in H_{m0} throughout the year and also within each month. Mean H_{m0} follows the progression of the seasons, with largest the waves occurring in the fall/winter months of November–January. Variability of H_{m0} within each month is also greatest November–January. Fig. 19 shows similar trends in J, with larger variability indicative of J's rough proportionality to H_{m0}^2. This large seasonal variation in J may be useful as it mimics the typical load demand of a BC coastal community.

Fig. 20 shows the variation of T_e through the year is relatively weak, ranging from 8 to 10 s. The variability of T_e within each month is also weak, with a nearly constant standard deviation of about 1.5 s. This low variability of wave period is a benefit for oscillating wave energy converters, which usually operate most efficiently near some design frequency.

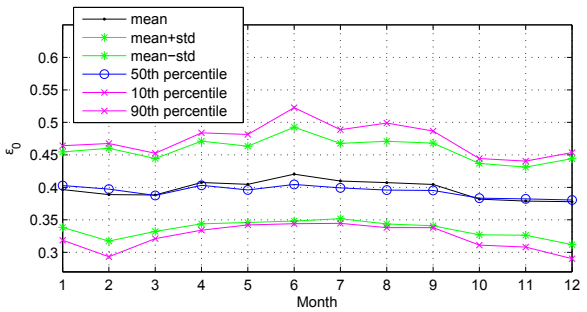

Fig. 21. Monthly variation of ε_0 at reference location.

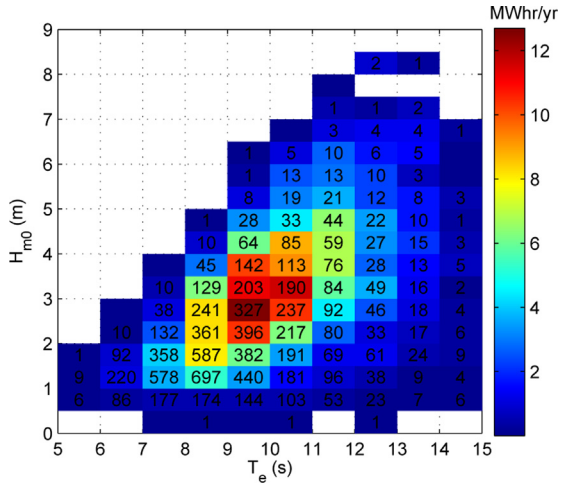

Fig. 22. Histogram showing the probability and energy distribution of sea-states in H_{m0}-T_e space. Colour contour show the cumulative energy in each bin for an average year. The numbers indicate the number of occurrences of sea-states in the given bin (as hours per year) for an average year. Occurrences are rounded to the nearest integer.

Fig. 21 shows a small seasonal variation of monthly mean ε_0. Lower values in occur in the winter due to strong storm swell and higher values occur in the summer due to predominant wind seas. Variation within each month is also low, but displays slight low bias in the winter and a slight high bias in the summer. Low variation in ε_0 is a benefit for oscillating wave energy converters as it allows the WEC to be designed with a constant response band-width.

In general the results found here agree well with other similar studies in the Eastern North Pacific [1,5,15].

6.3. Joint probability at reference location

The relationship between the joint probability of H_{m0} and T_e along with the associated wave energy is often important for WEC design. Fig. 22 shows both the frequency of occurrence and the accumulated wave energy for an average year at the reference location. It is interesting to note that the bin that contributes the largest amount of energy to the yearly total ($H_{m0} = 2.5–3.0$ m, $T_e = 9–10$ s) occurs less than half as often as the most frequently occurring combination of H_{m0} and T_e. For this particular site a WEC designer would have to consider designing for a device that produces consistent power, or designing for producing the maximum yearly output.

6.4. Comparison to wave energy test sites

Average yearly omni-directional wave power at the reference location is 31 kW/m. This value agrees well with the findings of a similar regional wave study [1]. The average wave power at the reference site near Hot Springs Cove is significantly greater than the estimated average yearly wave power at the WaveHub (18–20 kW/m) [16] or the 50 m berth at EMEC (24 kW/m) [17] and highlights the high potential for renewable wave energy development in the Hot Springs Cove area.

7. Conclusions

An assessment of the wave energy resources in the region around Hot Springs Cove has been presented. This work included the development of a near-shore wave propagation model using the REF/DIF-1 software running in linear mode. The model covers an area 37,000 m × 67,000 m at 50 m grid resolution. Model results were individually pre-computed for each wave component using a unit wave height. A transfer function approach was used to calculate wave spectra at each time step. Using NOAA WW3 directional spectra as boundary conditions, results were computed from March 2005 to February 2013.

The model results were parameterized to indicate the magnitude and frequency-direction distribution of energy within each sea-state. Yearly mean and monthly variation of wave parameters were used to indicate the spatial variability of the resource. A site in 50 m of water, appropriate for a 2-body point absorber, was selected based on a number of generic constraints and objectives. This site is used to illustrate the temporal variation of the spectral parameters within each month of the year.

The results indicate an energetic resource with significant variation of J in both space and time. Wave energy tends to concentrate at two shallower regions east and south of Hot Springs Cove. Monthly average J is about 6 times greater in the winter than the summer. T_e remains relatively constant in both space and time at about 8–10 s. Spectral width tends to be slightly larger during the predominant wind-seas of the summer and smaller during the swell typical of the winter, with little spatial variation. The wave power directionality coefficient d shows strong spatial consistency with an average value of about 87%.

Average yearly omni-directional wave power at the reference location is 31 kW/m. This is significantly greater than other major wave energy test sites in Europe such as the WaveHub (18–20 kW/m) and EMEC (24 kW/m). The strong directionally resolved wave resource, appropriate depth range and proximity to a financially motivated load-base make the region around Hot Springs Cove a good candidate for renewable wave energy development.

Acknowledgements

This work was completed as part of the West Coast Wave Initiative, a wave energy incubation program funded by Natural Resources Canada (RENE-082).

References

[1] Cornett A, Zhang J. Near-shore wave energy resources, western Vancouver island, B.C. Technical report CHC-TR-51. Canadian Hydraulic Centre; 2008.
[2] Iglesias G, Lpez M, Carballo R, Castro A, Fraguela J, Frigaard P. Wave energy potential in Galicia (NW Spain). Renew Energy 2009;34(11):2323–33. 0960–1481.
[3] Akpinar A, Komurcu Mh. Assessment of wave energy resource of the black sea based on 15-year numerical hindcast data. Appl Energy 2013;101(0):502–12. 0306–2619.
[4] van Nieuwkoop JC, Smith HC, Smith GH, Johanning L. Wave resource assessment along the Cornish coast (UK) from a 23-year hindcast dataset validated against buoy measurements. Renew Energy 2013;58(0):1–14. 0960–1481.
[5] Garcia-Medina G, Ozkan Haller HT, Ruggiero P. Wave resource assessment in Oregon and southwest Washington, USA. Renew Energy 2014;64(0):203–14. 0960–1481.
[6] Carballo R, Iglesias G. A methodology to determine the power performance of wave energy converters at a particular coastal location. Energy Convers Manag 2012;61(0):8–18. 0196–8904.
[7] Kirby JT, Dalrymple RA, Shi F. REF/DIF 1 v3.0 documentation and user's manual, center for applied coastal research. Newark, DE: Department of Civil and Environmental Engineering, University of Delaware; 2002. 19716, 3.0 edn.
[8] O'Reilly W, Guza R. A comparison of two spectral wave models in the southern California Bight. Coast Eng 1993;19(3–4):263–82. 0378–3839.
[9] Holthuijsen L. Waves in oceanic and coastal waters. Cambridge University Press; 2007.
[10] Folley M, Whittaker T. Analysis of the near-shore wave energy resource. Renew Energy 2009;34(7):1709–15. 0960–1481.
[11] Garcia-Medina G, Ozkan-Haller HT, Ruggiero P, Oskamp J. An inner-shelf wave forecasting system for the U.S. Pacific Northwest. Wea Forecasting 2013;28(3):681–703. 0882–8156.
[12] Fisheries and Oceans Canada. CSV format description; 2013. http://www.meds-sdmm.dfo-mpo.gc.ca/isdm-gdsi/waves-vagues/formats/csv-eng.htm.

[13] Durrant TH, Woodcock F, Greenslade DJM. Consensus forecasts of modeled wave parameters. Wea Forecasting 2009;24(2):492–503. 0882–8156.
[14] Folley M, Cornett A, Holmes B, Lenee-Bluhm P, Liria P. Standardising resource assessment for wave energy converters. In: The 4th International Conference on Ocean Energy; 2012.
[15] Lenee-Bluhm P, Paasch R, Ozkan Haller HT. Characterizing the wave energy resource of the US Pacific Northwest. Renew Energy 2011;36(8):2106–19. 0960–1481.
[16] Smith HC, Haverson D, Smith GH, Cornish CS, Baldock D. Assessment of the wave and current resource at the wave hub site. Tech. Rep. University of Exeter, Marine Energy Matters; 2011.
[17] Folley M, Elsaesser B, Whittaker T. Analysis of the wave Energy resource at the European Marine Energy Centre. In: Coasts, Marine Structures and Breakwaters Conference, Edinburgh; 2009.